IOP Publishing Biomed. Mater. 17 (2022) 025017 https://doi.org/10.1088/1748-605X/ac5673

Biomedical Materials

OPEN ACCESS

RECEIVED
28 September 2021

REVISED
28 December 2021

ACCEPTED FOR PUBLICATION
17 February 2022

PUBLISHED
1 March 2022

PAPER

Dual drug delivery collagen vehicles for modulation of skin fibrosis *in vitro*

João Q Coentro[1], Alessia di Nubila[1], Ulrike May[2], Stuart Prince[2], John Zwaagstra[3], Tero A H Järvinen[2,4] and Dimitrios I Zeugolis[1,5,*]

[1] Regenerative, Modular and Developmental Engineering Laboratory (REMODEL) and Science Foundation Ireland (SFI) Centre for Research in Medical Devices (CÚRAM), Biomedical Sciences Building, National University of Ireland Galway (NUI Galway), Galway, Ireland
[2] Faculty of Medicine and Health Technology, Tampere University, Tampere, Finland
[3] Human Health Therapeutics Research Centre, National Research Council Canada, Montreal, Quebec, Canada
[4] Tampere University Hospital, Tampere, Finland
[5] Regenerative, Modular and Developmental Engineering Laboratory (REMODEL), Charles Institute of Dermatology, Conway Institute of Biomolecular and Biomedical Research and School of Mechanical and Materials Engineering, University College Dublin (UCD), Dublin, Ireland
* Author to whom any correspondence should be addressed.

E-mail: dimitrios.zevgolis@ucd.ie

Keywords: collagen hydrogels, drug delivery, *in vitro* fibrosis model, scarring, antifibrotics

Supplementary material for this article is available online

Abstract

Single molecule drug delivery systems have failed to yield functional therapeutic outcomes, triggering investigations into multi-molecular drug delivery vehicles. In the context of skin fibrosis, although multi-drug systems have been assessed, no system has assessed molecular combinations that directly and specifically reduce cell proliferation, collagen synthesis and transforming growth factor β1 (TGFβ1) expression. Herein, a core–shell collagen type I hydrogel system was developed for the dual delivery of a TGFβ trap, a soluble recombinant protein that inhibits TGFβ signalling, and Trichostatin A (TSA), a small molecule inhibitor of histone deacetylases. The antifibrotic potential of the dual delivery system was assessed in an *in vitro* skin fibrosis model induced by macromolecular crowding (MMC) and TGFβ1. Sodium dodecyl sulphate-polyacrylamide gel electrophoresis (SDS-PAGE) and high performance liquid chromatography analyses revealed that ~50% of the TGFβ trap and ~30% of the TSA were released from the core and shell compartments, respectively, of the hydrogel system after 10 d (longest time point assessed) in culture. As a direct consequence of this slow release, the core (TGFβ trap)/shell (TSA) hydrogel system induced significantly ($p < 0.05$) lower than the control group (MMC and TGFβ1) collagen type I deposition (assessed via SDS-PAGE and immunocytochemistry), α smooth muscle actin (αSMA) expression (assessed via immunocytochemistry) and cellular proliferation (assessed via DNA quantification) and viability (assessed via calcein AM and ethidium homodimer-I staining) after 10 d in culture. On the other hand, direct TSA-TGFβ supplementation induced the lowest ($p < 0.05$) collagen type I deposition, αSMA expression and cellular proliferation and viability after 10 d in culture. Our results illustrate the potential of core–shell collagen hydrogel systems for sustained delivery of antifibrotic molecules.

Abbreviations

αSMA	α smooth muscle actin
ANOVA	analysis of variance
Col	collagen
C-S	core–shell modular hydrogel
DF	dermal fibroblasts
DAPI	4,6-diamidino-2-phenylindole
FITC	fluorescein isothiocyanate
HDACs	class I and II mammalian histone deacetylases
MMC	macromolecular crowding or crowder
NCL	non-crosslinked hydrogel
PBS	phosphate buffered saline

PEG	four arm polyethylene glycol succinimidyl glutarate
SDS-PAGE	sodium dodecyl sulphate-polyacrylamide gel electrophoresis
SMAD	small mothers against decapentaplegic
T122bt	TGFβ type II receptor-based trap
TGFβ	transforming growth factor β
TSAz	trichostatin A

1. Introduction

Considering that tissue development and growth and disease manifestation and progression are the result of multiple molecular and biological cascades, it is naïve to believe that single molecule therapeutic approaches will ever result in complete functional repair and regeneration. In this context, the use of multi-cargo delivery vehicles [1, 2] for a wide variety of clinical indications (e.g. ophthalmology [3], cancer [4], diabetic wounds [5], orthopaedics [6]) has been proposed. Data to-date, clearly illustrate the superiority of multi-molecular delivery systems over traditional mono-molecular administration approaches with respect to improved therapeutic effect, reduced systemic toxicity and lowered treatment cost [7–10].

Skin fibrosis is still an unmet clinical need, which affects (clinical outcomes range from cosmetic imperfections to functional impairment) over 100 million patients every year [11] and its associated annual healthcare expenditure in US alone exceeds US$ 12 billion [12]. Fibrotic skin disorders (e.g. scleroderma [13, 14], keloids and hypertrophic scars [15, 16]) are characterised by excessive and abnormal extracellular matrix (ECM) synthesis and deposition, which leads to altered tissue architecture and impaired function. Numerous cells, molecules and signalling pathways are involved in fibrosis manifestation, progression and exacerbation during the three (inflammatory, proliferative and remodelling) phases of the jeopardised wound healing process [17–19], rendering it a prime target for multi-molecular delivery. In a clinical setting, intralesional multi-molecular therapies have shown improved patient outcomes in comparison to their mono-molecular counterparts [20–25], but the mode of administration offers little control over cargo protection, localisation and bioavailability [26, 27] and the use of steroids as one of the molecular treatment modalities is often associated with numerous side effects (e.g. toxicity, pain, ulceration, atrophy) [28–31].

In the quest of the ideal carrier for localised and sustained delivery of multiple therapeutics, the use of hydrogels [32, 33] and electrospun scaffolds [34, 35] has been advocated for efficiency, simplicity and scalability purposes across all clinical indications. In hypertrophic and keloid scars, various electrospun and hydrogel dual-delivery systems (e.g. antimetabolite/glucocorticoid [36]; antioxidant/glucocorticoid [37]; anti-inflammatory/pro-wound healing [38]; cell proliferation and activation regulator/anti-inflammatory [39] combinations) have clearly demonstrated promise (details of the studies are provided in supplementary table S1 (available online at stacks.iop.org/BMM/17/025017/mmedia)). However, despite the notable results that these proof-of-principle studies have demonstrated, one cannot but note that no study has yet assessed molecular combinations that are directly and specifically involved in reducing cell proliferation, collagen synthesis and expression of TGFβ1, the major orchestrator of fibrosis [40–42].

Considering the above, herein, we ventured to develop a differentially crosslinked collagen-based multi-compartment hydrogel system for dual drug delivery. We selected pepsin extracted and PEG crosslinked collagen due to its well established cytocompatibility, low macrophage response and reduced antigenicity and immunogenicity [43–49]. Further, collagen-based devices have long history in wound management, including chronic wound management [50–53]. TSA, a HDAC inhibitor, was chosen, due to its well-established history in suppressing collagen synthesis, preventing TGFβ1 signalling, inducing fibrotic cell apoptosis, suppressing myofibroblast activation and augmenting M2 macrophage polarisation [54–57]. Similarly, a TGFβ trap was used as a second molecule, as it has been shown to reduce cell proliferation; small mothers against decapentaplegic (SMAD 2) phosphorylation; TGFβ1 induced collagen expression and synthesis; and connective tissue growth factor expression [58–61]. The efficiency and effectiveness of the produced dual delivery hydrogels systems to supress fibrosis were assessed in the improved *in vitro* scar model [62–64] that utilises TGFβ1 to induce fibroblast transformation to myofibroblast, which is associated with de novo αSMA expression and increased collagen synthesis [65–67] and MMC to increase collagen deposition [68–70].

2. Materials and methods

2.1. Materials

All plasticware were obtained from Sarstedt (Ireland) and Thermo Fisher Scientific (Ireland). All chemicals and reagents were purchased from Sigma–Aldrich (Ireland), unless otherwise stated. Porcine Achilles tendons were obtained from a local slaughterhouse.

2.2. Collagen type I extraction and purification

Collagen type I was extracted using the acid/pepsin digestion method [71, 72]. Briefly, using a sterile surgical scalpel, surrounding fascia and fat were removed and the tendons were cut in small pieces

(1 × 1 × 1 cm). After freezing at −80 °C, the tendon pieces were cryo-milled into a powder using liquid nitrogen and a Freezer/Mill 6870 (SPEX SamplePrep, USA). The tendon powder was repeatedly washed with PBS and then suspended in 1 M ethanoic acid solution for 48 h at 4 °C. Pepsin (porcine gastric mucosa, 3200–4500 units mg^{-1} protein, catalogue number: P6887) was then added into the solution for further 48 h at 4 °C. The collagen suspension was then sieved, filtered and purified by repeated salt precipitation (0.9 M NaCl), centrifugation (11 000 g for 20 min) and 1 M ethanoic acid re-solubilisation at 4 °C. The collagen solution was then dialysed against 0.05 M ethanoic acid and stored at 4 °C. The purity of the final atelocollagen solution (5 mg ml^{-1}) was determined by SDS-PAGE [73] and correlated to purified collagen type I (Symatese, France). Briefly, the extracted collagen and the Symatese obtained collagen were neutralised with 1 M NaOH, denatured at 95 °C and resolved under non-reducing conditions using in-house a 5% resolving and a 3% stacking polyacrylamide gels on a Mini-Protean 3 (Bio-Rad Laboratories, UK) system. The gels were stained with a SilverQuest™ Silver Staining Kit (Invitrogen, Ireland) according to the manufacturer's instructions. The in-house extracted collagen preparation exhibited a typical collagen type I electrophoretic mobility, comparable to the commercially available collagen type I (supplementary figure S1).

2.3. Fabrication of multi-compartment collagen type I hydrogels

Core–shell collagen hydrogels were produced in a stepwise process in ice, unless specified otherwise at specific steps (figure 1 and supplementary table S2). Firstly, the bottom part of the shell compartment was prepared by mixing the atelocollagen solution with 10× PBS, 1 M NaOH and 0.5 mM or 1 mM PEG (final concentration, JenKem Technology, USA); centrifuging to remove air bubbles; and gelling for 2 h at 37 °C. After gelling, a polylactic acid 3D-printed cubical mould (height: 2.05, 3 or 5 mm; width: 2.05, 3 or 5 mm; depth: 2.05, 3 or 5 mm) was centred on top of the bottom part of the shell compartment and a mixture of atelocollagen, 10× PBS, 1 M NaOH and 0.5 mM or 1 mM PEG (final concentration) was added up to the rim of the mould. After gelling for 2 h at 37 °C, the mould was carefully removed and the core compartment was formed by pouring in the void of the removed mould a mixture of atelocollagen, 10× PBS, 1 M NaOH and 1 mM or 2 mM PEG (final concentration) and letting it gel for 2 h at 37 °C. Afterwards, the top part of the shell compartment was formed by adding a mixture of atelocollagen, 10× PBS, 1 M NaOH and 0.5 mM or 1 mM PEG (final concentration) and letting it gel for 2 h at 37 °C, resulting in the formation of a multi-compartment core–shell hydrogel. Different crosslinking densities for each compartment (1 mM shell compartment and 2 mM core compartment) were selected in an attempt to develop a hydrogel system with sequential drug release capacity.

2.4. FITC release assay

A solution of FITC-dextran (40 kDa) in PBS, at an initial concentration of 5 mg ml^{-1} was added to the core compartment of the 0.5 mM PEG shell/1 mM PEG core and 1 mM PEG shell/2 mM PEG core hydrogels at the time of their formation for a final concentration of 200 μg ml^{-1}. After gelling, the hydrogels were immersed in 1 ml PBS. Aliquots of 100 μl were removed at the appropriate time points (0, 0.04, 0.08, 0.17, 0.33, 1, 2, 3, or 7 d) and replaced with fresh PBS. Quantification of cumulative released FITC-dextran was assessed through the measurement of fluorescence at 495 nm (Varioskan Flash, Thermo Fisher Scientific, USA).

2.5. Mechanical compression analysis

The 1 mM PEG shell/2 mM PEG core hydrogels (8 mm diameter and 8 mm thick) were subjected to compression testing using a biaxial mechanical testing equipment (ZwickRoell, Germany), operating as follows: loading speed of 5 mm min^{-1}, maximum displacement of 50% and maximum applied force of 10 N. The compression modulus was calculated as the slope from the linear elastic behaviour region of the plotted stress–strain curve. As a control, NCL, fabricated in a single step process (i.e. non-modular), were used. These hydrogels were prepared in the same type of containers as the core–shell hydrogels by mixing the atelocollagen solution with 10× PBS, neutralising it with NaOH, homogenising the resulting solution and incubating it for 16 h at 37 °C to promote gelation.

2.6. Cell culture, induction of fibrosis and antifibrotic effect analysis

Normal adult dermal fibroblasts (DF, PCS-201-012, ATCC, USA) were cultured in media containing high glucose DMEM (4500 mg l^{-1} glucose, L-glutamine, sodium pyruvate and sodium bicarbonate), 10% foetal bovine serum and 1% penicillin–streptomycin at 37 °C in a humidified atmosphere of 5% CO_2. Cells were routinely sub-cultured and trypsinised at 80% confluence and used between passages 3 and 6, with medium changes every 2 and 3 d. To induce fibrosis, 25 000 cells cm^{-2} were seeded in 24 or 48-well plates and after 24 h, the media changed to media containing 100 μM L-ascorbic acid 2-phosphate sesquimagnesium salt hydrate, 100 μg ml^{-1} 500 kDa dextran sulphate, the MMC agent used, and 5 ng ml^{-1} TGFβ1 [63]. Core–shell hydrogels, loaded with antifibrotic compounds during the fabrication process (3 μM TSA and 150 nM T122bt [74] at the shell and core compartments, respectively) were added to the cells at the same time as the MMC/TGFβ1 media change and cultured for 4, 7 and 10 d. The same molecules (at

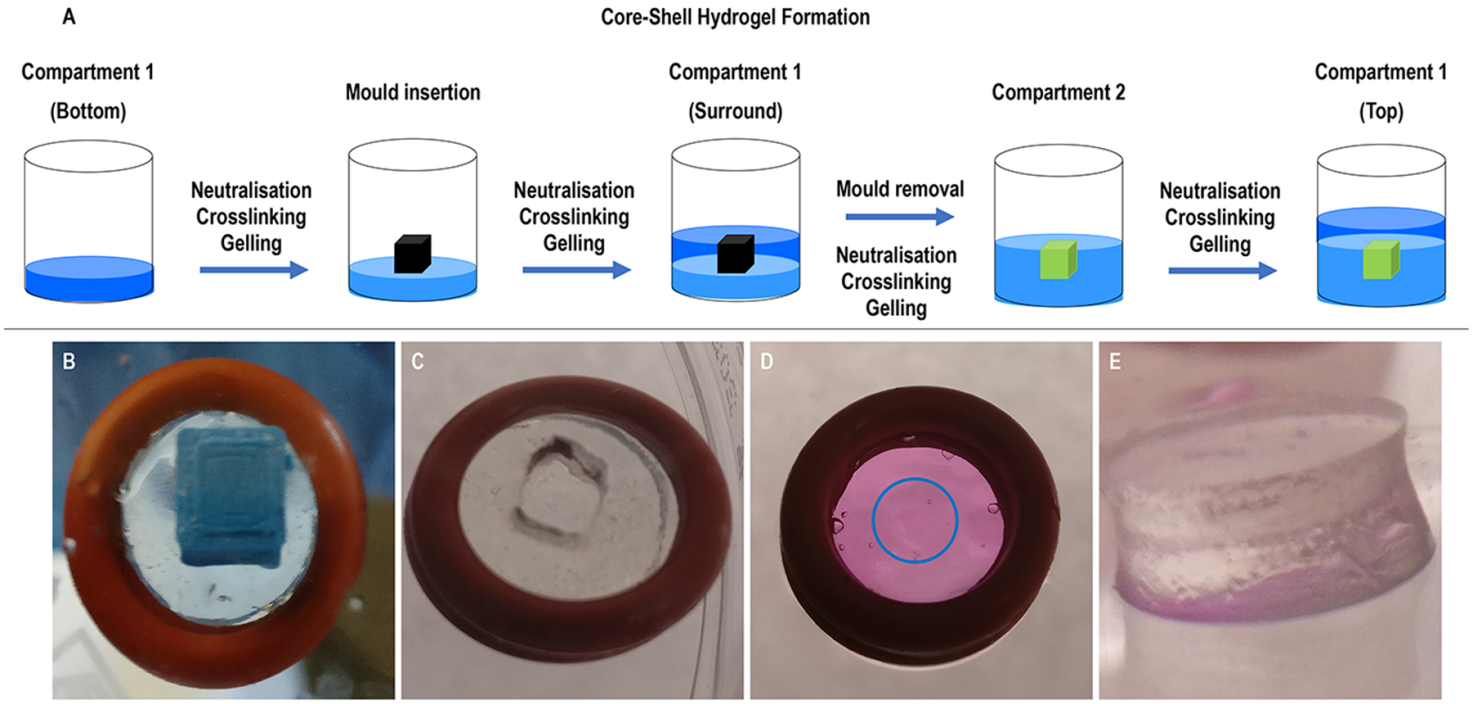

Figure 1. (A) Schematic of the formation process of the core–shell multi-compartment collagen hydrogel system using porcine Achilles tendon collagen type I solution, crosslinked with different concentrations of PEG and loaded with different anti-fibrotic substances on each compartment. (B) Optimisation of the production of the core–shell multi-compartment collagen type I hydrogels in O-rings—insertion of a PDMS-coated 3D-printed PLA mould on top of the gelled bottom collagen type I hydrogel layer in an O-ring. (C) Removal of the mould for the creation of an inner compartment in the hydrogel system. (D) Complete multi-compartment hydrogel system in an O-ring with the inner compartment (highlighted with a blue circle). (E) Side view of the complete hydrogel system when removed from the O-ring support.

1 μM and 50 nM, respectively) were also added directly to the media (alone and together), to act as positive control groups. Media were changed every 3 d and read outs were obtained after 4, 7 and 10 d.

2.7. TSA and T122bt release assays

A solution of TSA was added to the shell compartment of the 1 mM PEG shell/2 mM PEG core hydrogels at the time of their formation for a final concentration of 3 μM. A solution of T122bt was added to the core compartment of the 1 mM PEG shell/2 mM PEG core hydrogels at the time of their formation for a final concentration of 150 nM. After gelling, the core–shell hydrogels were added to the cells under the induced fibrotic model, immersed in 0.5 ml of complete media and cultured for up to 10 d. Aliquots of 100 μl were removed at 0, 1 and 2 d, while at days 4, 7 and 10, 250 μl were removed and replaced with fresh complete culture media. Quantification of cumulative released TSA and T122bt were assessed through high performance liquid chromatography (HPLC) and SDS-PAGE, respectively.

Regarding TSA, quantification was performed using a Shimadzu Prominence-I LC-2030 Plus (Shimadzu Corporation, Japan). Chromatographic separation was achieved through an InfinityLab Poroshell 120 SB-C18 column (4.6 mm × 150 mm; 2.7 μm, Agilent, USA) with two mobile phases, A and B. As previously reported in the literature [75], mobile phase A was prepared as a 0.1% v/v orthophosphoric acid solution, while mobile phase B as a acetonitrile solution with a linear gradient program. This program was implemented by achieving certain ratios of mobile phase B at predetermined times [min/% B: 0/10, 7/65, 8/10 and 12/40], while using a 10.0 μl injection volume and maintaining a flow rate of 0.6 ml min^{-1} and the column temperature at 25 °C. Standard and sample solutions were prepared using a diluent solution (water, acetonitrile and formic acid at a ratio of 65:35:0.1). Samples were then detected and quantified at 272 nm and data were analysed with the Shimadzu LabSolutions CS software (Shimadzu Corporation, Japan).

As for T122bt quantification, at the appropriate time points, culture media was aspirated, the remnants of the collagen systems were removed and cell supernatant was analysed by SDS-PAGE as described elsewhere [73], with adapted polyacrylamide percentages. Briefly, culture media were aspirated, denatured at 95 °C and resolved under non-reducing conditions using in-house resolving and stacking polyacrylamide gels (12% and 6%, respectively) on a Mini-Protean 3 (Bio-Rad Laboratories, UK) system. Samples were stained using a SilverQuest™ Silver Staining Kit (Invitrogen, Ireland) according to the manufacturer's instructions. T122bt release was quantified through densitometric analysis of the present T122bt SDS-PAGE bands using ImageJ software (NIH, USA).

2.8. Electrophoresis analysis

At each time point, the cell culture media and the collagen hydrogels were removed and the cell layers were analysed by SDS-PAGE [73]. Briefly, the cell layers were washed with PBS and digested with 0.1 mg ml^{-1} pepsin solution (porcine gastric mucosa, 3500–4200 U mg^{-1}, catalogue number: P6887) in 0.5 M acetic acid. The cell layers were then scraped, neutralised with 1 M NaOH, denatured at 95 °C and resolved under non-reducing conditions using in-house resolving and stacking polyacrylamide gels (5% and 3%, respectively) on a Mini-Protean 3 (Bio-Rad Laboratories, UK) system. Purified collagen type I (Symatese, France) was used as standard. Samples were stained using a SilverQuest™ Silver Staining Kit (Invitrogen, Ireland) according to the manufacturer's instructions. Densitometric analysis was performed for α1(I), α2(I), β11(I), β12(I) or γ(I) bands, as appropriate, using ImageJ software (NIH, USA) and collagen concentration was normalised to DNA quantity.

2.9. Immunocytochemistry analysis

At each time point, the cell culture media and the collagen hydrogels were removed, the cells were washed with PBS for 5 min, fixed with 4% paraformaldehyde in PBS at pH 7.4 for 15 min at room temperature and washed three times with PBS for 5 min each time. For intracellular markers, cells were permeabilised with 0.25% Triton X-100 in PBS for 10 min and then washed three times with PBS for 5 min each time. Cells were then blocked with 5%–7.5% donkey serum in PBS for 1 h at room temperature, after which they were incubated with primary antibody (rabbit anti-human collagen type I, 1:300, PA2140-2, Boosterbio, USA; mouse anti-human αSMA, 1:300, ab7817, Abcam, UK; rabbit anti-human collagen type III, 1:300, ab7778, Abcam, UK) for either 90 min (Col I and αSMA) at room temperature or overnight at 4 °C (Col III). Samples were then washed three times with PBS and incubated with secondary antibodies (Alexa Fluor™ 594 donkey anti-rabbit, 1:500, R37119 or Alexa Fluor™ 488 goat anti-mouse, 1:400, A-11 001; both from Thermo Fisher Scientific, USA) for 60 min at room temperature. Cell nuclei were counterstained with DAPI for 5 min at room temperature and samples were washed three times with PBS. Samples were then imaged with an inverted fluorescence microscope (Olympus IX-81, Olympus Corporation, Japan) and further processed with ImageJ software (NIH, USA).

2.10. Cell proliferation analysis

The Quant-iT™ PicoGreen™ dsDNA Assay Kit (Invitrogen, USA) was used to quantify DNA concentration as per the manufacturer's instructions. Briefly, at each time point, the cell culture media and the collagen hydrogels were removed, the cells were washed with PBS for 5 min, ultrapure water was added and

three cycles of freezing at −80 °C and thawing at 37 °C to promote cell lysis were conducted. A range (0.2–4 μg ml^{-1}) of standard DNA concentrations in ultrapure water was prepared. Samples and standards were mixed with 10 mM Tris-HCl and 1 mM ethylenediaminetetraacetic acid buffer (pH 7.5) and PicoGreen™ reagent and incubated in the dark for 5 min at room temperature. Fluorescence was measured at 480 nm excitation and 520 nm emission with a Varioskan Flash Spectral scanning multimode reader (Thermo Fisher Scientific, USA).

2.11. Cell metabolic activity analysis

Cell metabolic activity was quantified using the alamarBlue® Cell Viability assay (Thermo Fisher Scientific, USA) as per the manufacturer's instructions. Briefly, at each time point, the cell culture media and the collagen hydrogels were removed, the cells were washed with PBS for 5 min and incubated with a 10% alamarBlue® solution in PBS for 3 h at 37 °C in a humidified atmosphere of 5% CO_2. Absorbance was then measured at 550 nm and 595 nm with a Varioskan Flash Spectral scanning multimode reader (Thermo Scientific, USA). Cell metabolic activity was expressed on terms of percentage reduction of the alamarBlue® dye and normalised to DNA content and to the non-treated control.

2.12. Cell viability analysis

Cell viability was assessed using staining with calcein AM (live cell marker, Invitrogen, USA) and ethidium homodimer I (dead cell marker, Invitrogen, USA). Briefly, at each time point, the cell culture media and the collagen hydrogels were removed, the cells were carefully washed with PBS and incubated with a solution of 4 μM calcein AM and 2 μM ethidium homodimer I in PBS for 30 min at 37 °C in a humidified atmosphere of 5% CO_2. Cells were then imaged with an inverted fluorescence microscope Olympus IX-81 (Olympus Corporation, Japan), using the FITC filter for calcein AM and the Texas Red filter for ethidium homodimer and further processed with ImageJ software (NIH, USA).

2.13. Statistical analysis

Statistical evaluation of the data was performed using MiniTab® version 17 (Minitab Inc., USA). All data are expressed as mean value ± standard deviation. Datasets were assessed for normal distribution (Anderson–Darling test) and equal variance (Bartlett's and Levene's test for homogeneity of variances). When either or both assumptions were violated, non-parametric analysis was conducted using Kruskall–Wallis test for multiple comparisons and Mann–Whitney U test for pairwise comparisons. For samples that were confirmed to follow both parametric analysis assumptions, one-way ANOVA was used for multiple comparisons and Tukey's post hoc test was used for pairwise comparisons. Statistical significance was accepted at $p < 0.05$.

3. Results

3.1. FITC-dextran release analysis

Quantification of released FITC-dextran revealed that the 0.5 mM PEG shell/1 mM PEG core hydrogel released ∼80% of FITC-dextran within 2 d, whilst the 1 mM PEG shell/2 mM PEG core hydrogel released ∼30% of FITC-dextran after 7 d (supplementary figure S2). For this reason, the 1 mM PEG shell/2 mM PEG core hydrogel was chosen for further analysis.

3.2. Biomechanical analysis

Compression testing analysis (table 1) revealed that PEG crosslinking significantly ($p < 0.05$) increased stress at failure and compression modulus of both compartments and significantly ($p < 0.05$) reduced strain at failure of the shell compartment. Typical stress–strain curves for collagen-based materials, characterised by the presence of both elastic and plastic deformation behaviour were obtained (supplementary figure S3).

3.3. Antifibrotic release and effect analyses

SDS-PAGE and HPLC quantification revealed that core (T122bt)-shell (TSA) hydrogels promoted a sustained release of the encapsulated cargos over time, resulting in 27.72% ± 1.98% of released TSA and 51.51% ± 20.94% of released T122bt after 10 d, which equates to concentrations of 0.83 ± 0.06 μM and 77.27 ± 31.41 nM in the media (figures 2 and S4).

Starting with collagen deposition via SDS-PAGE and complementary densitometric quantification of α(I)1 and α(I)2 chains (figure 3), it revealed that at day 4, the core–shell and core (T122bt)-shell groups induced significantly ($p < 0.05$) higher collagen deposition than the +MMC + TGFβ1 group. At day 7, all core–shell hydrogel groups induced significantly ($p < 0.05$) lower collagen deposition than the +MMC + TGFβ1 group. At day 10, all groups except the core–shell and T122bt alone induced significantly ($p < 0.05$) lower collagen deposition than the +MMC + TGFβ1 group. At the same time point, the core–shell (TSA), core (T122bt)-shell and TSA-T122bt alone groups also induced significantly ($p < 0.05$) lower collagen deposition than the core–shell group. Among all drug groups, at day 7, the core–shell (TSA) hydrogel group and at day 10, the TSA-T122bt alone group induced the lowest collagen deposition, in comparison to the +MMC + TGF group ($p < 0.05$). No significant ($p > 0.05$) changes in the deposition of β11(I), β12(I) dimers and γ(I) trimers were observed (supplementary figure S5).

Immunocytochemistry (figure 4(A)) and complementary image intensity analysis (figure 4(B)) made apparent that among all drug groups, at day

Table 1. Comparison testing biomechanical analysis of NCL non-core–shell hydrogels and crosslinked core–shell modular hydrogels. Statistical analysis through one-way ANOVA and Tukey's post-hoc comparison test or Kruskal Wallis and Mann Whitney post-hoc analysis where appropriate, +: indicates significant ($p < 0.05$) increase. #: indicates significant ($p < 0.05$) decrease. $n = 6$.

		Stress at failure (kPa)	Strain at failure (mm mm^{-1})	Compression modulus (kPa)
NCL, non-core–shell hydrogel		4.9 ± 1.6	0.38 ± 0.06	16.6 ± 4.2
Core–shell hydrogel	Shell 1 mM PEG	8.2 ± 1.9 +	0.28 ± 0.03 #	57.8 ± 21.8 +
	Core 2 mM PEG	13.2 ± 4.8 +	0.42 ± 0.04	88.8 ± 47.6 +

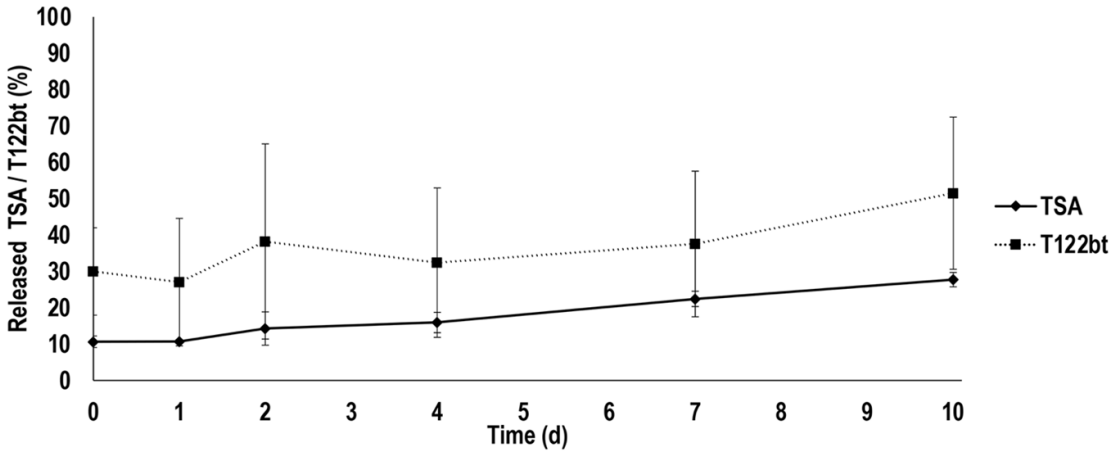

Figure 2. Core (T122bt)-shell (TSA) hydrogels promoted a sustained release of TSA and T122bt over time. Release profile over time of TSA (shell) and T122bt (core) enclosed in a core–shell hydrogel system and crosslinked with 1 (shell) and 2 (core) mM PEG placed on top of cultured DF and submerged under complete culture media. The hydrogel systems resulted in an approximate release of 28% and 52% of TSA and T122bt, respectively ($n = 3$ and 4).

7 the TSA alone group and at day 10 the TSA alone group and the TSA-T122bt alone group induced the lowest ($p < 0.05$) collagen type I deposition, in comparison to the +MMC + TGF group.

Immunocytochemistry (figure 5(A)) and complementary image intensity analysis (figure 5(B)) made apparent that no significant ($p < 0.05$) differences were observed in collagen type III expression between any of the drug groups and the +MMC + TGF group, while at day 7 the core (T122bt)-shell (TSA) and TSA alone groups significantly ($p < 0.05$) decreased its deposition when compared to the core–shell group.

Immunocytochemistry (figure 6(A)) and complementary image intensity analysis (figure 6(B)) made apparent that among all drug groups, at day 4, the TSA alone group and the TSA-T122bt alone group; at day 7, the core (T122bt)-shell (TSA) hydrogel group, the TSA alone group and the TSA-T122bt alone group; and at day 10, the TSA alone group and the TSA-T122bt alone group induced the lowest ($p < 0.05$) αSMA expression, all in comparison to the +MMC + TGF group.

With respect to basic cellular function analysis, at day 4, the TSA-T122bt alone group and at day 7 and day 10, the shell (TSA) hydrogel group and the TSA-T122bt alone group induced the lowest ($p < 0.05$) DNA concentration (figure 7(A)). The shell (TSA) hydrogel group induced the highest metabolic activity at day 7 and day 10 (figure 7(B)). Treatment with TSA alone at day 4 and TSA-T122bt alone at all time points decreased cell viability, which was ameliorated when delivered through the core (T122bt)-shell (TSA) system (figure 8).

Confocal microscopy showed that DFs migrated into the collagen hydrogels during the treatment period, presenting a lower viability in the hydrogels containing TSA (supplementary figure S6).

4. Discussion

Considering the fibrosis is a multi-stage process, it is unlikely that single-molecule therapies will lead to functional therapeutic outcomes. Although intralesional injections of multiple molecules are extensively used in clinical practice, the mode of administration offers little control over the cargos' protection, localisation and bioavailability, which has triggered investigation into vehicle-based multi-delivery systems. Considering the above, herein we developed and characterised a core (loaded with a TGFβ trap)/shell (loaded with TSA) collagen type I hydrogel system and assessed its antifibrotic potential in an *in vitro* fibrosis model.

Collagen crosslinking with PEG significantly improved the biomechanical and drug release

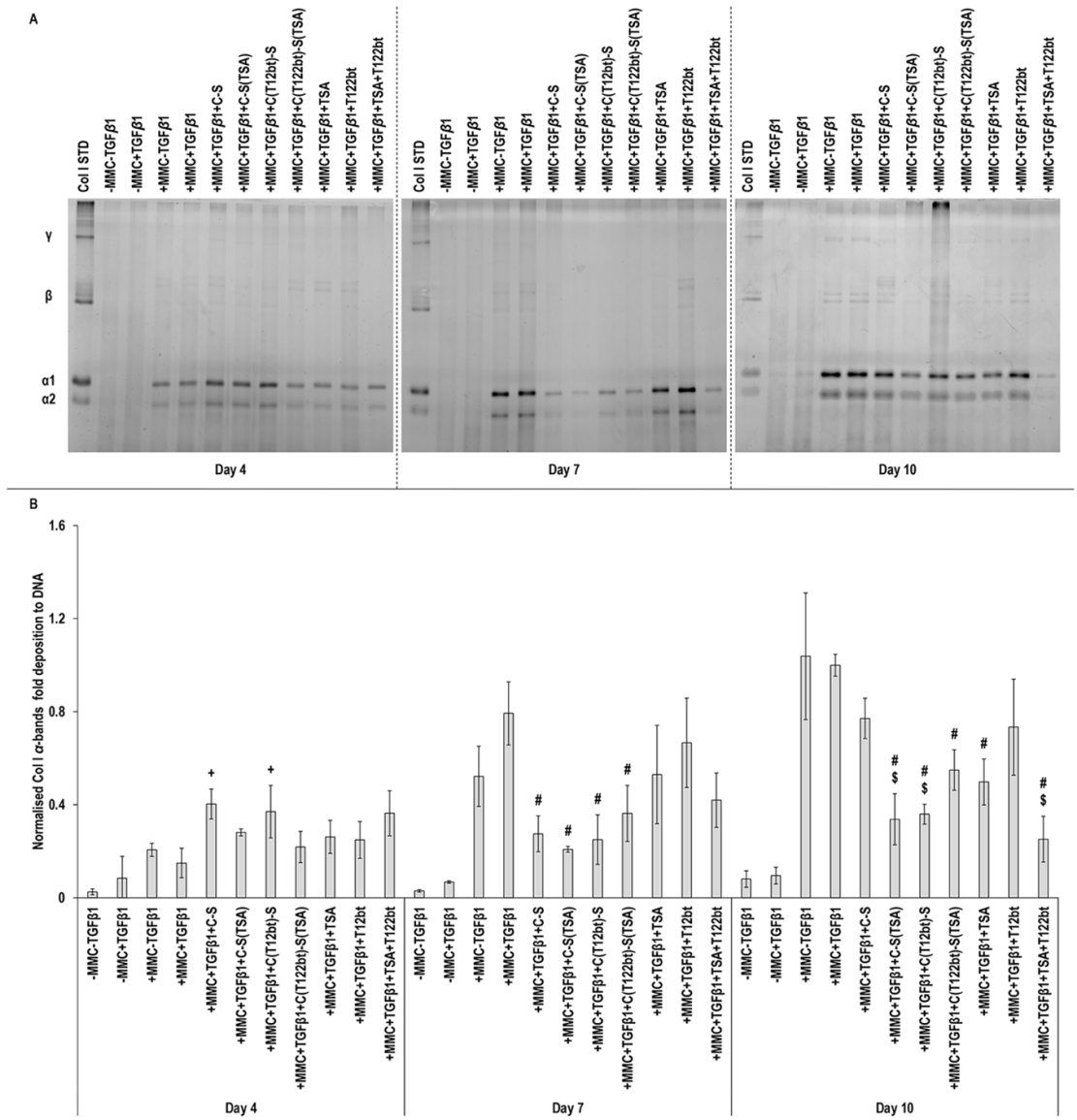

Figure 3. Treatment with antifibrotic-loaded hydrogels affects collagen type I deposition. The dual delivery of TSA and T122bt through the core–shell collagen hydrogel resulted in a decrease of deposited collagen type I at days 7 and 10. The C-S(TSA); C(T122bt)-S and C(T122bt)-S(TSA) groups at day 7 and the C-S(TSA), C(T122bt)-S and the TSA-T122bt alone groups at day 10 induced the lowest collagen type I deposition in comparison to the +MMC + TGFβ1 group, as revealed by SDS-PAGE (A) and densitometry of α(I)1 and α(I)2 bands (B). Col I STD: 0.1 mg ml^{-1}. Statistical analysis through one-way ANOVA and Tukey's post-hoc comparison test, + indicates a statistically significant increase compared to the +MMC + TGFβ1 group of the same time point, # indicates a statistically significant decrease compared to the +MMC + TGFβ1 group of the same time point, $ indicates a statistically significant decrease compared to the +MMC + TGFβ1 + C-S group of the same time point, $p < 0.05$ ($n = 3$).

properties of the produced hydrogels. Starting with biomechanical analysis, the collagen hydrogels showed a typical stress–strain curve of semi-crystalline polymers that experience both elastic and plastic deformation [76, 77]. Crosslinking resulted in increased resistance to mechanical forces, as has been well-documented previously in the literature with PEG crosslinked collagen fibres [45, 78], films [46, 47, 79], sponges [80, 81] and hydrogels [44, 82], as well as gelatin hydrogels [83] and scleral collagen [84]. Moving into molecular loading and release, crosslinking restrained the release of the encapsulated FITC-dextran, TSA and T122bt, which can be attributed to the resultant tight molecular structure that increases resistance to degradation and slows down the diffusion process [85–90]. With respect to the release profile capacity, ~10% and 30% of the TSA was released from the shell after 1 and 10 d, respectively, and ~30% of the TGFβ1 trap was released from the core within the 1st day and the same level of release was maintained for up to 10 d. We recognise that the TGFβ1 trap exhibited a rather burst release at the beginning, which we attribute to the fabrication method, during which some of the water-soluble TGFβ1 trap was diffused from the core layer to the shell layer and from there was released to the media. The same issue has been reported previously in the literature when a

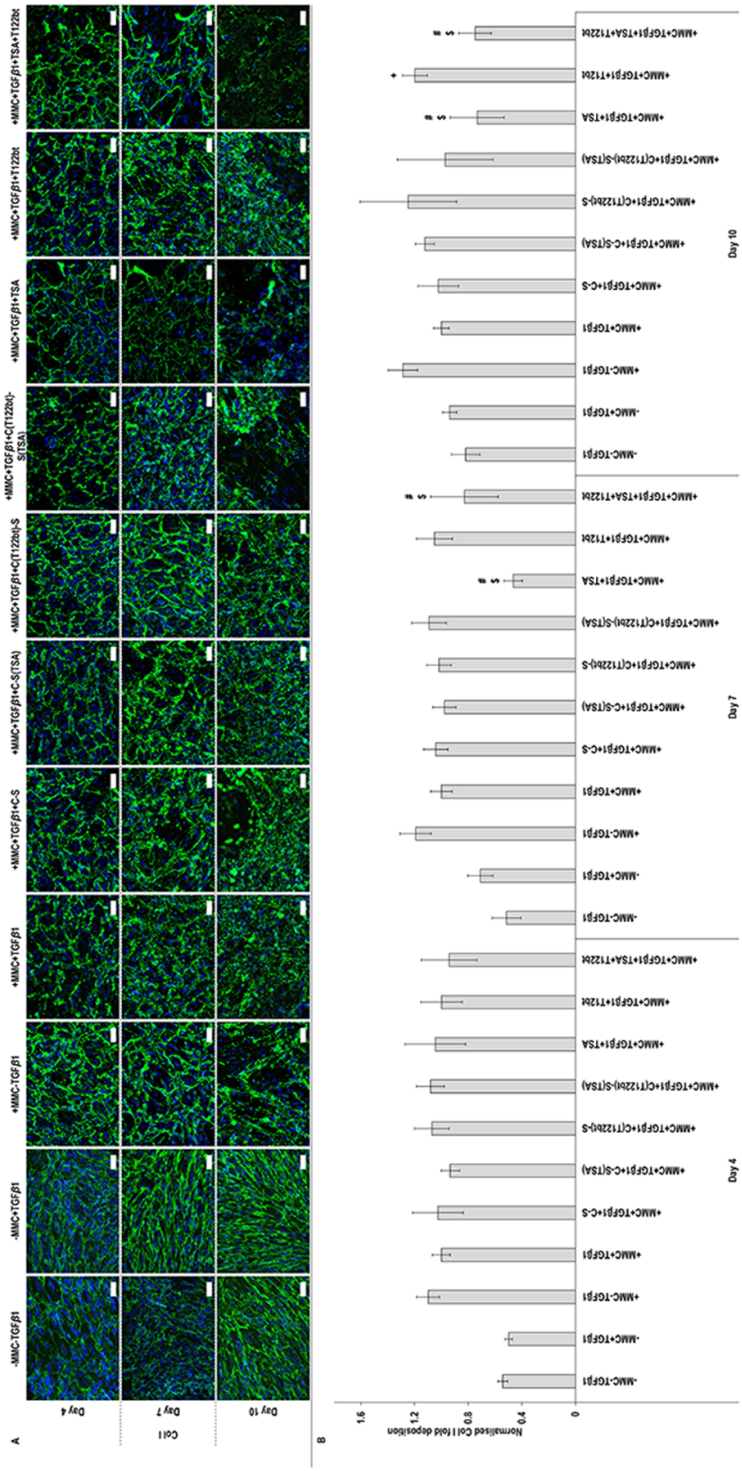

Figure 4. Treatment with antifibrotic-loaded hydrogels and antifibrotic drugs alone affects collagen type I deposition. Immunocytochemistry (A) and image intensity analyses (B) revealed no differences in collagen type I deposition between the groups at day 4, while the TSA group alone induced the highest decrease at days 7 and 10 when compared to the +MMC + TGFβ1 group ($p < 0.05$). Scale bar: 100 µm. Kruskal Wallis and Mann Whitney post-hoc analysis were conducted, + indicates a statistically significant increase compared to the +MMC + TGFβ1 group of the same time point, # indicates a statistically significant decrease compared to the +MMC + TGFβ1 group of the same time point, $ indicates a statistically significant decrease compared to the C-S group of the same time point, $p < 0.05$ ($n = 3$).

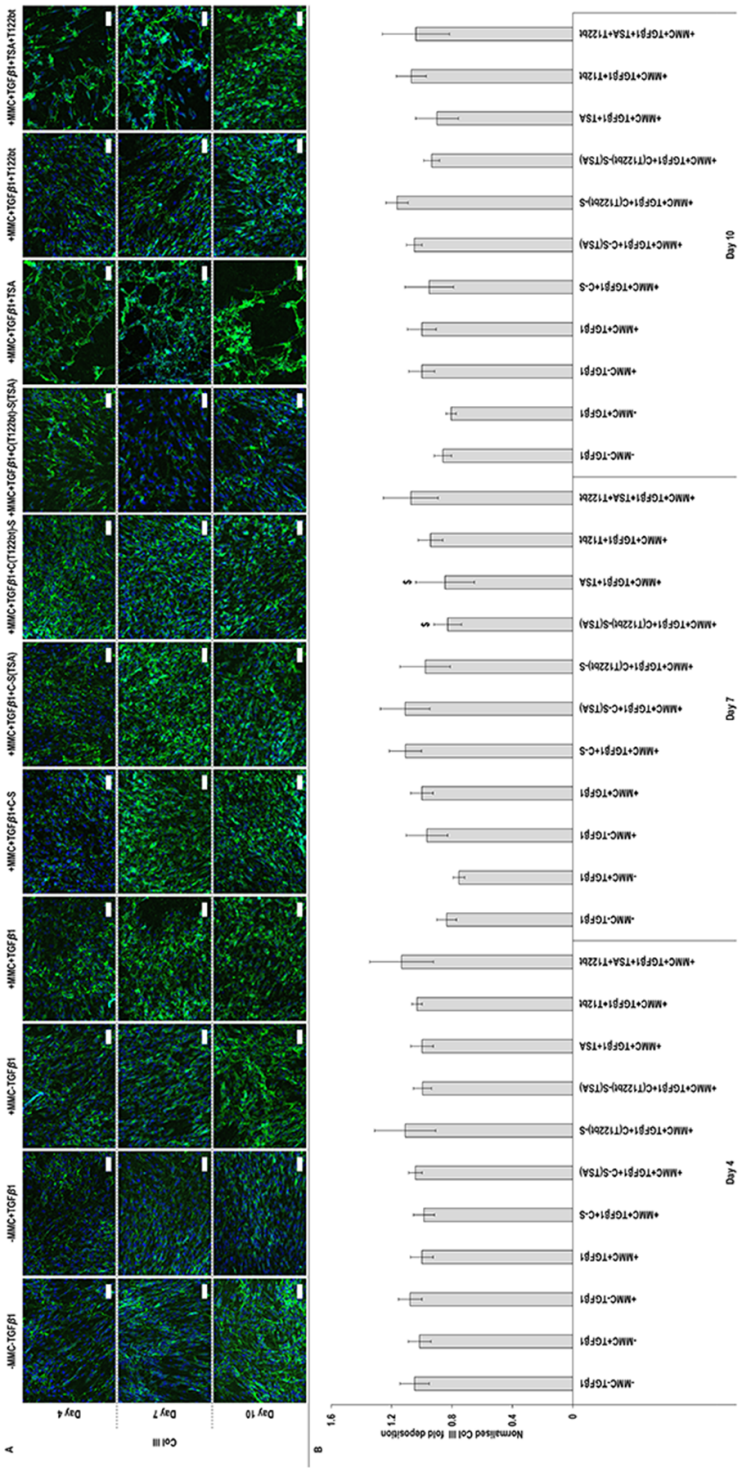

Figure 5. Different treatments did not affect collagen type III expression when compared to the +MMC + TGFβ1 group. Immunocytochemistry (A) and image intensity analyses (B) revealed no differences were observed in collagen type III expression between the groups at all time points when compared to the +MMC + TGFβ1 group, while the core (T122bt)-shell (TSA) group induced a significant difference when compared with the C-S group at day 7 ($p < 0.05$). Scale bar: 100 µm. One-way ANOVA and Tukey's post-hoc comparison test or Kruskal Wallis and Mann Whitney post-hoc analysis were conducted. $ indicates a statistically significant decrease compared to the core–shell group of the same time point, $p < 0.05$ ($n = 3$).

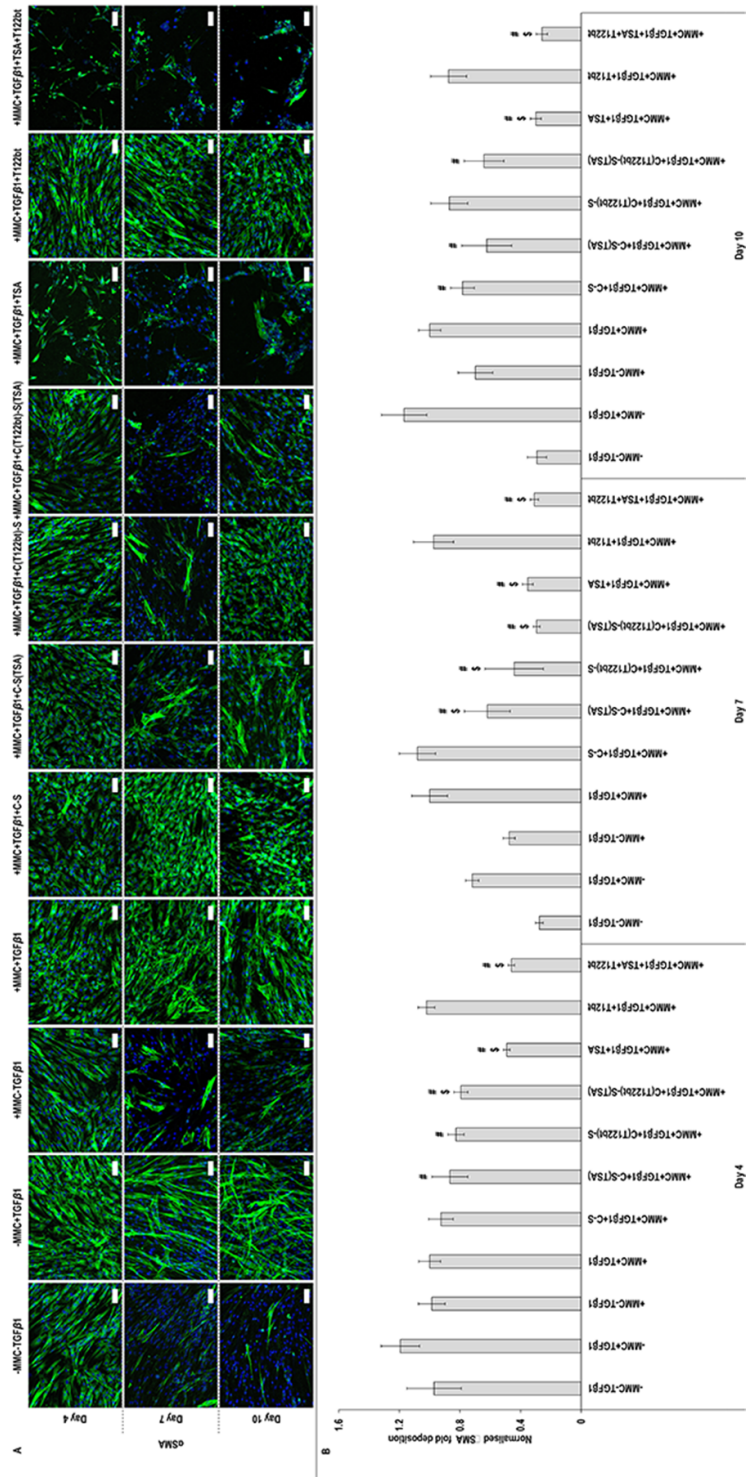

Figure 6. Treatment with core (T122bt)-shell (TSA), TSA and TSA-T122bt alone resulted in the highest decrease in αSMA expression. Immunocytochemistry (A) and image intensity analyses (B) revealed that TSA and TSA-T122b alone induced the highest decrease in αSMA expression at day 4, while at day 7 this was observed for the core (T122bt)-shell (TSA), TSA and TSA-T122bt alone groups and at day 10 for the TSA and TSA-T122bt groups when compared to the +MMC + TGFβ1 group ($p < 0.05$). The core (T122bt)-shell (TSA) group also resulted in a decrease in αSMA expression at all time points when compared to the +MMC + TGFβ1 ($p < 0.05$). Scale bar: 100 μm. One-way ANOVA and Tukey's post-hoc comparison test or Kruskal Wallis and Mann Whitney post-hoc analysis were conducted, + indicates a statistically significant increase compared to the +MMC + TGFβ1 group of the same time point, # indicates a statistically significant decrease compared to the +MMC + TGFβ1 group of the same time point, $ indicates a statistically significant decrease compared to the C-S group of the same time point, $p < 0.05$ ($n = 3$).

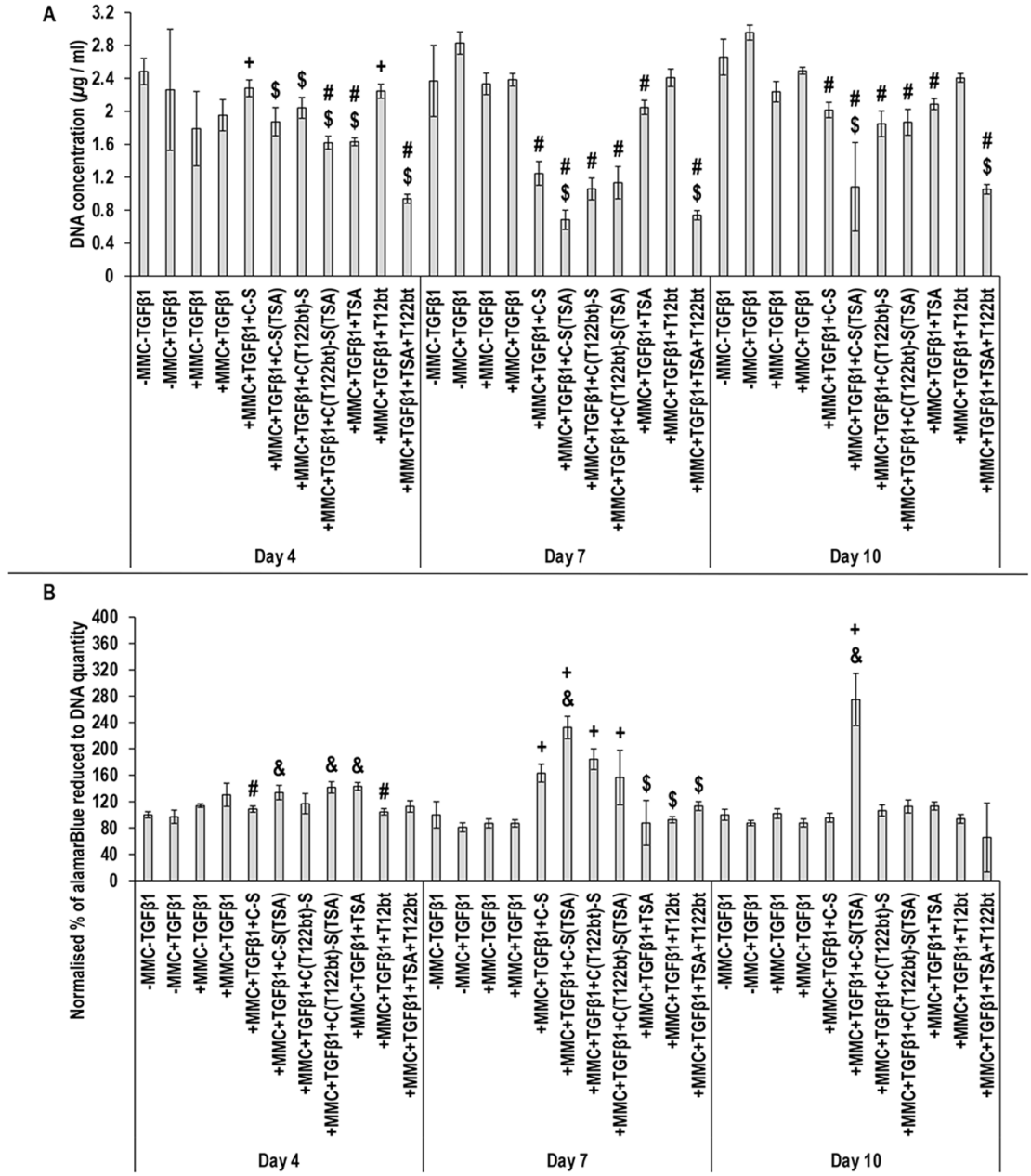

Figure 7. Treatment with an antifibrotic encapsulating modular hydrogel ameliorates the effect on cell proliferation and metabolic activity compared to supplementation with the drugs alone. Analysis of cell proliferation (PicoGreen™) (A) and normalised metabolic activity to DNA quantity (alamarBlue™) (B) after 4, 7 and 10 d in culture and supplementation with +MMC + TGFβ1 and different combinations of TSA, T122bt and a C-S hydrogel system. Treatment with TSA-T122bt alone resulted in the highest decrease of cell proliferation, which was alleviated when delivered through the hydrogel system ($p < 0.05$). C-S(TSA) resulted in the highest increase in metabolic activity at days 7 and 10, which was also reduced when coupled with T122bt ($p < 0.05$). Statistical analysis through one-way ANOVA and Tukey's post-hoc comparison test or Kruskal Wallis and Mann Whitney post-hoc analysis where appropriate, + indicates a statistically significant increase compared to the +MMC + TGFβ1 group of the same time point, # indicates a statistically significant decrease compared to the +MMC + TGFβ1 group of the same time point, & indicates a statistically significant increase compared to the +MMC + TGFβ1 + C-S group of the same time point, $ indicates a statistically significant decrease compared to the +MMC + TGFβ1 + C-S group of the same time point, $p < 0.05$ ($n = 3$).

double-layer alginate-carboxymethyl cellulose hydrogel system was used [91]. It is worth noting that similar bioactive/therapeutic molecules release profiles from crosslinked collagen scaffolds have been observed over the years (details of indicative examples are provided in supplementary table S3). We feel that appropriate one-step multi-compartment scaffold fabrication, crosslinking density optimisation and/or affinity/covalent-based drug incorporation may offer more accurate pharmacokinetics of the encapsulated cargos.

When the produced collagen hydrogel system was put to the test in the *in vitro* fibrosis model, an increased at the early time point (day 4), followed by a decreased at the later time points (day 7 and day 10) collagen deposition was detected. We attribute the initial (day 4) collagen increase to the collagen hydrogel degradation, which may have occurred due

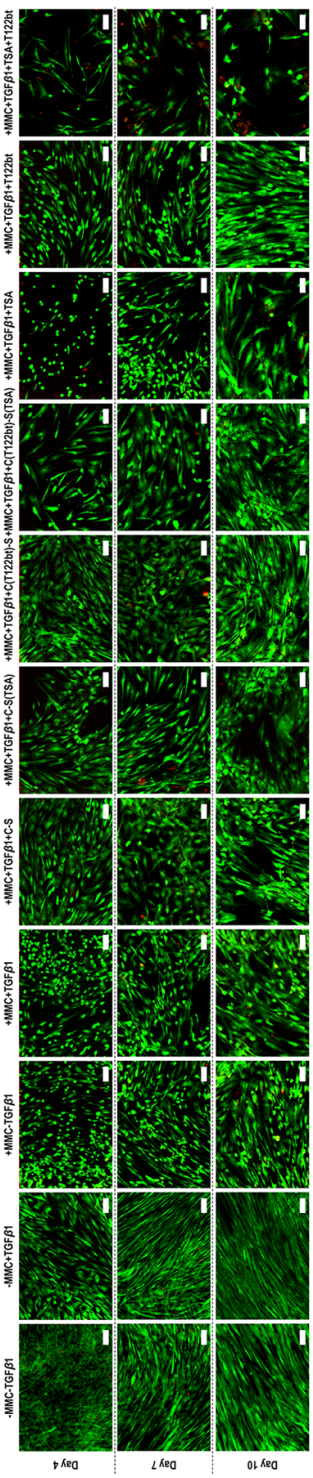

Figure 8. Treatment with an antifibrotic encapsulating C-S hydrogel ameliorates the decrease on cell viability compared to supplementation with the drugs alone. Analysis of cell viability through calcein AM (green, viable cells) and ethidium homodimer (red, non-viable cells) fluorescence staining after 4, 7 and 10 d in culture and supplementation with +MMC + TGFβ1 and with different combinations of hydrogels, TSA and T122bt. Treatment with TSA alone at day 4 and TSA-T122bt alone at all time points decreased cell viability, which was ameliorated when delivered through the core (T122bt)-shell (TSA) system. Scale bar: 100 µm ($n = 3$).

to the action of secreted [17, 92] and media present [93] matrix metalloproteinases. Some chemoprotection of the TGFβ1 by the collagen hydrogel cannot be excluded as well, considering the strong affinity of TGFβ1 to collagen scaffolds [94] and that TGFβ1 has a half-time ranging from 2 to 100 min [95], which can be prolonged when bound to ECM molecules [96] or synthetic molecules, such as PEG [97]. At later time points (day 7 and day 10), although treatment with TGFβ trap on its own was not enough to elicit a significant decrease in collagen deposition and while TSA proved to be effective in that regard, we observed substantial additive effect when the molecules were delivered in tandem through the core–shell hydrogel system. In line with the inhibition on collagen type I expression, we also detected a reduction in myofibroblasts with the combination of TSA and TGFβ trap in the core–shell hydrogel. Both these observations validate our hypothesis, considering that TSA is an inhibitor of HDACs, which alters gene expression by altering the access of transcription factors to DNA; reduces myofibroblast transformation, collagen deposition and cellular proliferation; and promotes cellular apoptosis in experimental skin fibrosis models [54–56]. TGFβ1, in turn, is a key growth factor in many fibrotic conditions [41], due to its role in transforming fibroblasts into myofibroblasts and increasing collagen type I deposition [98, 99], and as such, a TGFβ1 trap constitutes a therapeutic agent of interest in the treatment and prevention of skin fibrosis. In addition to fibrosis modulation, it is also worth pointing out that the dual delivery of TSA and T122bt through the hydrogel system had a beneficial cellular function effect compared to monomolecular delivery or no-carrier delivery approaches. These data therefore further support the notion of combination approach to inhibit and/or restrain fibrosis, as it has been documented previously (supplementary table S1).

Considering the innate complexity (multiple cells, molecules and spatiotemporal events) of wound healing, combinational therapies are continuously gaining pace in clinical practice, especially in difficult to heal wounds (e.g. diabetic wound healing [100–104], burns [101, 105–108], hypertrophic scars and keloids [20–25]). The beneficial effects of single-compartment/dual delivery vehicles have been well established in the wound healing literature for simultaneous delivery of therapeutics [109–112]. Better understanding of biological processes coupled with recent advancements in biomaterials engineering (e.g. layer-by-layer [113–115], core–shell [116–118]) now allow for the development of multi-compartment and multi-delivery vehicles for sustained, localised and overlapping/sequential delivery of bioactive/therapeutic molecules for a diverse range of clinical indications. In this spirit, herein we developed a core–shell collagen hydrogel system for overlapping/sequential release of TSA from the shell and a TGFβ1 trap from the core in order to supress cell proliferation and simultaneously or subsequently supress αSMA expression and collagen synthesis. Pharmacokinetics analysis revealed that using a collagen hydrogel system that allows for molecular diffusion, overlapping release of the TSA and the TGFβ1 trap ($\sim$30%) in the 1st 10 d (longest time point assessed) was observed. For sequential release, more potent, but still cytocompatible, crosslinking methods (supplementary table S3) for the core compartment should be assessed. It is also worth noting that the developed hydrogels retained their structural stability for 10 d in culture (longest time point assessed) and similar systems have been shown to maintain their integrity and cargo release capacity for up to 16 weeks in preclinical setting without any notable side effects (supplementary table S4), clearly illustrating the clinical relevance of the produced system.

5. Conclusions

Contemporary drug delivery systems aspire to target simultaneously multiple signalling pathways for functional therapeutic outcomes. Multi-molecular therapies are progressively gaining pace in scar-wars, considering the number of cells, molecules and signalling pathways involved in fibrosis manifestation, progression and establishment. In this context, we developed a core (loaded with a TGFβ trap)/shell (loaded with TSA) collagen type I hydrogel system, the antifibrotic capacity of which was assessed in an *in vitro* fibrosis model. Our data illustrate that the core–shell hydrogel system allowed for sustained release of the antifibrotic molecules, resulting in significant decrease, in comparison to the control group, in collagen type I deposition, αSMA expression and cellular proliferation and viability. On the other hand, direct TGFβ trap and TSA supplementation induced the lowest collagen type I deposition, αSMA expression and cellular proliferation and viability. Our data further support the use of multi-compartment and multi-delivery systems for sustained delivery of antifibrotic molecules.

Data availability statement

The data that support the findings of this study are available upon reasonable request from the authors.

Acknowledgments

The authors want to thank Mrs Marianne Karlsberg for recombinant protein expression and purification.

Conflict of interest

J Z is the owner of the TGFβ trap of the study. J Q C, A D N, U M, S P, T A H J and D I Z declare no conflict of interest. The funders had no role in the design; in

the collection, analyses, or interpretation of data; in the writing of the manuscript, or in the decision to publish the results.

Author contributions

J Q C, T A H J, D I Z Methodology: J Q C, A D N, U M, S P, J Z Data analysis: J Q C. Manuscript writing and editing: J Q C, T A H J, D I Z. Final manuscript approval: All authors.

Funding

This work has received funding from the European Research Council (ERC) under the European Union's Horizon 2020 research and innovation programme, Grant Agreement No. 866126. This publication has emanated from research supported in part by grants from Science Foundation Ireland (SFI) under Grant Numbers 15/CDA/3629 and 19/FFP/6982 and Science Foundation Ireland (SFI) and European Regional Development Fund (ERDF) under Grant Number 13/RC/2073_2. This research was also funded by the Finnish National Agency for Education (EDUFI), Academy of Finland, Päivikki and Sakari Sohlberg Foundation, Tampere Tuberculosis Foundation, Tampere University Hospital Research Fund and Pirkanmaa Hospital District Research Foundation.

ORCID iD

Dimitrios I Zeugolis https://orcid.org/0000-0002-7599-5191

References

[1] Pugliese E, Coentro J Q and Zeugolis D I 2018 Advancements and challenges in multidomain multicargo delivery vehicles *Adv. Mater.* **30** e1704324
[2] He C, Tang Z, Tian H and Chen X 2016 Co-delivery of chemotherapeutics and proteins for synergistic therapy *Adv. Drug Deliv. Rev.* **98** 64–76
[3] Mahaling B, Baruah N, Ahamad N, Maisha N, Lavik E and Katti D S 2021 A non-invasive nanoparticle-based sustained dual-drug delivery system as an eyedrop for endophthalmitis *Int. J. Pharm.* **606** 120900
[4] Qiu Y, Bai J, Feng Y, Shi X and Zhao X 2021 Use of pH-active catechol-bearing polymeric nanogels with glutathione-responsive dissociation to codeliver bortezomib and doxorubicin for the synergistic therapy of cancer *ACS Appl. Mater. Interfaces* **13** 36926–37
[5] Wang Y, Wu Y, Long L, Yang L, Fu D, Hu C, Kong Q and Wang Y 2021 Inflammation-responsive drug-loaded hydrogels with sequential hemostasis, antibacterial, and anti-inflammatory behavior for chronically infected diabetic wound treatment *ACS Appl. Mater. Interfaces* **13** 33584–99
[6] Wang P, Perche F, Midoux P, Cabral C S D, Malard V, Correia I J, Ei-Hafci H, Petite H, Logeart-Avramoglou D and Pichon C 2021 *In vivo* bone tissue induction by freeze-dried collagen-nanohydroxyapatite matrix loaded with BMP2/NS1 mRNAs lipopolyplexes *J. Control. Release* **334** 188–200
[7] Yu S, He C and Chen X 2018 Injectable hydrogels as unique platforms for local chemotherapeutics-based combination antitumor therapy *Macromol. Biosci.* **18** e1800240
[8] Poustchi F, Amani H, Ahmadian Z, Niknezhad S, Mehrabi S, Santos H and Shahbazi M 2021 Combination therapy of killing diseases by injectable hydrogels: from concept to medical applications *Adv. Healthcare Mater.* **10** e2001571
[9] Yang Z, Gao D, Cao Z, Zhang C, Cheng D, Liu J and Shuai X 2015 Drug and gene co-delivery systems for cancer treatment *Biomater. Sci.* **3** 1035–49
[10] Carvalho B, Vit F, Carvalho H, Han S and de la Torre L 2021 Recent advances in co-delivery nanosystems for synergistic action in cancer treatment *J. Mater. Chem.* B **9** 1208–37
[11] Sund B and Arrow A K 2000 New developments in wound care, clinica reports
[12] Griffin M F, Desjardins-Park H E, Mascharak S, Borrelli M R and Longaker M T 2020 Understanding the impact of fibroblast heterogeneity on skin fibrosis *Dis. Model Mech.* **13** dmm044164
[13] Cutolo M, Soldano S and Smith V 2019 Pathophysiology of systemic sclerosis: current understanding and new insights *Expert Rev. Clin. Immunol.* **15** 753–64
[14] Varrica C, Dias H, Reis C, Carvalheiro M and Simões S 2021 Targeted delivery in scleroderma fibrosis *Autoimmun. Rev.* **20** 102730
[15] Wang Z, Zhao W, Cao Y, Liu Y, Sun Q, Shi P, Cai J, Shen X and Tan W 2020 The roles of inflammation in keloid and hypertrophic scars *Front. Immunol.* **11** 603187
[16] Kumar A and Kamalasanan K 2021 Drug delivery to optimize angiogenesis imbalance in keloid: a review *J. Control. Release* **329** 1066–76
[17] Coentro J Q, Pugliese E, Hanley G, Raghunath M and Zeugolis D I 2018 Current and upcoming therapies to modulate skin scarring and fibrosis *Adv. Drug Deliv. Rev.* **146** 37–59
[18] Russo B, Brembilla N and Chizzolini C 2020 Interplay between keratinocytes and fibroblasts: a systematic review providing a new angle for understanding skin fibrotic disorders *Front. Immunol.* **11** 648
[19] Dees C, Chakraborty D and Distler J 2021 Cellular and molecular mechanisms in fibrosis *Exp. Dermatol.* **30** 121–31
[20] Koc E, Arca E, Surucu B and Kurumlu Z 2008 An open, randomized, controlled, comparative study of the combined effect of intralesional triamcinolone acetonide and onion extract gel and intralesional triamcinolone acetonide alone in the treatment of hypertrophic scars and keloids *Dermatol. Surg.* **34** 1507–14
[21] Lee J H, Kim S E and Lee A Y 2008 Effects of interferon-alpha2b on keloid treatment with triamcinolone acetonide intralesional injection *Int. J. Dermatol.* **47** 183–6
[22] Sharma S, Vinay K and Bassi R 2021 Treatment of small keloids using intralesional 5-fluorouracil and triamcinolone acetonide versus intralesional bleomycin and triamcinolone acetonide *J. Clin. Aesthet. Dermatol.* **14** 17–21 (https://www.ncbi.nlm.nih.gov/pmc/articles/PMC8021404/)
[23] Darougheh A, Asilian A and Shariati F 2009 Intralesional triamcinolone alone or in combination with 5-fluorouracil for the treatment of keloid and hypertrophic scars *Clin. Exp. Dermatol.* **34** 219–23
[24] Morelli Coppola M, Salzillo R, Segreto F and Persichetti P 2018 Triamcinolone acetonide intralesional injection for the treatment of keloid scars: patient selection and perspectives *Clin. Cosmet. Invest. Dermatol.* **11** 387–96
[25] Camacho-Martínez F, Rey E, Serrano F and Wagner A 2013 Results of a combination of bleomycin and triamcinolone acetonide in the treatment of keloids and hypertrophic scars *An. Bras. Dermatol.* **88** 387–94

[26] Wang W, Lu K, Yu C, Huang Q and Du Y 2019 Nano-drug delivery systems in wound treatment and skin regeneration *J. Nanobiotechnol.* **17** 82
[27] Kim H, Sun X, Lee J, Kim H, Fu X and Leong K 2019 Advanced drug delivery systems and artificial skin grafts for skin wound healing *Adv. Drug Deliv. Rev.* **146** 209–39
[28] Méndez-Echevarría A, Fernandez-Prieto A, de la Serna O, Lopez-Gutierrez J, Parron M, Marin-Aguilera B and Calvo C 2018 Acute lung toxicity after intralesional bleomycin sclerotherapy *Pediatrics* **141** e20161787
[29] Huang C, Liu L, You Z, Du Y and Ogawa R 2019 Managing keloid scars: from radiation therapy to actual and potential drug deliveries *Int. Wound J.* **16** 852–9
[30] Trisliana Perdanasari A, Lazzeri D, Su W, Xi W, Zheng Z, Ke L, Min P, Feng S, Zhang Y and Persichetti P 2014 Recent developments in the use of intralesional injections keloid treatment *Arch. Plast. Surg.* **41** 620–9
[31] Zhuang Z, Li Y and Wei X 2021 The safety and efficacy of intralesional triamcinolone acetonide for keloids and hypertrophic scars: a systematic review and meta-analysis *Burns* **47** 987–98
[32] Wei Z, Volkova E, Blatchley M and Gerecht S 2019 Hydrogel vehicles for sequential delivery of protein drugs to promote vascular regeneration *Adv. Drug Deliv. Rev.* **149–150** 95–106
[33] Tang R, Liu Z, Gu S and Liu X 2021 Multiple local therapeutics based on nano-hydrogel composites in breast cancer treatment *J. Mater. Chem.* B **9** 1521–35
[34] Jeckson T, Neo Y, Sisinthy S and Gorain B 2021 Delivery of therapeutics from layer-by-layer electrospun nanofiber matrix for wound healing: an update *J. Pharm. Sci.* **110** 635–53
[35] Bhattarai R, Bachu R, Boddu S and Bhaduri S 2018 Biomedical applications of electrospun nanofibers: drug and nanoparticle delivery *Pharmaceutics* **11** 5
[36] Bao Z, Gao P, Xia G, Wang Z, Kong M, Feng C, Cheng X, Liu Y and Chen X 2016 A thermosensitive hydroxybutyl chitosan hydrogel as a potential co-delivery matrix for drugs on keloid inhibition *J. Mater. Chem.* B **4** 3936–44
[37] Li J, Fu R, Li L, Yang G, Ding S, Zhong Z and Zhou S 2014 Co-delivery of dexamethasone and green tea polyphenols using electrospun ultrafine fibers for effective treatment of keloid *Pharm. Res.* **31** 1632–43
[38] Cheng L, Sun X, Zhao X, Wang L, Yu J, Pan G, Li B, Yang H, Zhang Y and Cui W 2016 Surface biofunctional drug-loaded electrospun fibrous scaffolds for comprehensive repairing hypertrophic scars *Biomaterials* **83** 169–81
[39] Zhang N, Gao T, Wang Y, Liu J, Zhang J, Yao R and Wu F 2020 Modulating cationicity of chitosan hydrogel to prevent hypertrophic scar formation during wound healing *Int. J. Biol. Macromol.* **154** 835–43
[40] Ye Z and Hu Y 2021 TGF-β1: gentlemanly orchestrator in idiopathic pulmonary fibrosis (review) *Int. J. Mol. Med.* **48** 132
[41] Lodyga M and Hinz B 2020 TGF-β1—a truly transforming growth factor in fibrosis and immunity *Semin. Cell Dev. Biol.* **101** 123–39
[42] Budi E, Schaub J, Decaris M, Turner S and Derynck R 2021 TGF-β as a driver of fibrosis: physiological roles and therapeutic opportunities *J. Pathol.* **254** 358–73
[43] Sorushanova A *et al* 2019 The collagen suprafamily: from biosynthesis to advanced biomaterial development *Adv. Mater.* **31** 1801651
[44] Collin E, Grad S, Zeugolis D, Vinatier C, Clouet J, Guicheux J, Weiss P, Alini M and Pandit A 2011 An injectable vehicle for nucleus pulposus cell-based therapy *Biomaterials* **32** 2862–70
[45] Sanami M *et al* 2016 The influence of poly(ethylene glycol) ether tetrasuccinimidyl glutarate on the structural, physical, and biological properties of collagen fibers *J. Biomed. Mater. Res.* B **104** 914–22
[46] Delgado L M, Fuller K and Zeugolis D I 2017 Collagen cross-linking: biophysical, biochemical, and biological response analysis *Tissue Eng.* A **23** 1064–77
[47] Delgado L, Fuller K and Zeugolis D 2018 Influence of cross-linking method and disinfection/sterilization treatment on the structural, biophysical, biochemical, and biological properties of collagen-based devices *ACS Biomater. Sci. Eng.* **4** 2739–47
[48] Delgado L, Bayon Y, Pandit A and Zeugolis D 2015 To cross-link or not to cross-link? Cross-linking associated foreign body response of collagen-based devices *Tissue Eng.* B **21** 298–313
[49] Lynn A, Yannas I and Bonfield W 2004 Antigenicity and immunogenicity of collagen *J. Biomed. Mater. Res.* B **71** 343–54
[50] Chattopadhyay S and Raines R 2014 Review collagen-based biomaterials for wound healing *Biopolymers* **101** 821–33
[51] Gould L 2016 Topical collagen-based biomaterials for chronic wounds: rationale and clinical application *Adv. Wound Care* **5** 19–31
[52] Sharma S, Rai V, Narang R and Markandeywar T Collagen-based formulations for wound healing: a literature review *Life Sci.* accepted (https://pubmed.ncbi.nlm.nih.gov/34715138/)
[53] Mathew-Steiner S, Roy S and Sen C 2021 Collagen in wound healing *Bioengineering* **8** 63
[54] Rombouts K *et al* 2002 Trichostatin A, a histone deacetylase inhibitor, suppresses collagen synthesis and prevents TGF-beta(1)-induced fibrogenesis in skin fibroblasts *Exp. Cell Res.* **278** 184–97
[55] Diao J S, Xia W S, Yi C G, Wang Y M, Li B, Xia W, Liu B, Guo S Z and Sun X D 2011 Trichostatin A inhibits collagen synthesis and induces apoptosis in keloid fibroblasts *Arch. Dermatol. Res.* **303** 573–80
[56] Huber L C *et al* 2007 Trichostatin A prevents the accumulation of extracellular matrix in a mouse model of bleomycin-induced skin fibrosis *Arthritis Rheumatol.* **56** 2755–64
[57] Tseng W, Tsai M, Chen N and Tarng D 2020 Trichostatin A alleviates renal interstitial fibrosis through modulation of the M2 macrophage subpopulation *Int. J. Mol. Sci.* **21** 5966
[58] Varricchio L *et al* 2021 TGF-β1 protein trap AVID200 beneficially affects hematopoiesis and bone marrow fibrosis in myelofibrosis *JCI Insight* **6** e145651
[59] Chu Y, Guo F, Li Y, Li X, Zhou T and Guo Y 2008 A novel truncated TGF-beta receptor II downregulates collagen synthesis and TGF-beta I secretion of keloid fibroblasts *Connect. Tissue Res.* **49** 92–98
[60] Wong C, Falkenham A, Myers T and Légaré J 2018 Connective tissue growth factor expression after angiotensin II exposure is dependent on transforming growth factor-β signaling via the canonical smad-dependent pathway in hypertensive induced myocardial fibrosis *J. Renin Angiotensin Aldosterone Syst.* **19** 1470320318759358
[61] Stepien D *et al* 2020 Tuning macrophage phenotype to mitigate skeletal muscle fibrosis *J. Immunol.* **204** 2203–15
[62] Coentro J Q, May U, Prince S, Zwaagstra J, Ritvos O, Järvinen T A H and Zeugolis D I 2021 Adapting the scar-in-a-jar to skin fibrosis and screening traditional and contemporary anti-fibrotic therapies *Front. Bioeng. Biotechnol.* **9** 756399
[63] Chen C Z C, Peng Y X, Wang Z B, Fish P V, Kaar J L, Koepsel R R, Russell A J, Lareu R R and Raghunath M 2009 The scar-in-a-jar: studying potential antifibrotic compounds from the epigenetic to extracellular level in a single well *Br. J. Pharmacol.* **158** 1196–209
[64] Rønnow S *et al* 2020 Prolonged scar-in-a-jar: an *in vitro* screening tool for anti-fibrotic therapies using biomarkers of extracellular matrix synthesis *Respir. Res.* **21** 108
[65] Tuan T, Song A, Chang S, Younai S and Nimni M 1996 *In vitro* fibroplasia: matrix contraction, cell growth, and

collagen production of fibroblasts cultured in fibrin gels *Exp. Cell Res.* **223** 127–34
[66] Clark R, McCoy G, Folkvord J and McPherson J 1997 TGF-beta 1 stimulates cultured human fibroblasts to proliferate and produce tissue-like fibroplasia: a fibronectin matrix-dependent event *J. Cell. Physiol.* **170** 69–80
[67] Fish P *et al* 2007 Potent and selective nonpeptidic inhibitors of procollagen C-proteinase *J. Med. Chem.* **50** 3442–56
[68] Zeugolis D 2021 Bioinspired *in vitro* microenvironments to control cell fate: focus on macromolecular crowding *Am. J. Physiol. Cell Physiol.* **320** C842–49
[69] Raghunath M and Zeugolis D 2021 Transforming eukaryotic cell culture with macromolecular crowding *Trends Biochem. Sci.* **46** 805–11
[70] Tsiapalis D and Zeugolis D 2021 It is time to crowd your cell culture media—physicochemical considerations with biological consequences *Biomaterials* **275** 120943
[71] Delgado L M, Shologu N, Fuller K and Zeugolis D I 2017 Acetic acid and pepsin result in high yield, high purity and low macrophage response collagen for biomedical applications *Biomed. Mater.* **12** 065009
[72] Zeugolis D I, Paul R G and Attenburrow G 2008 Factors influencing the properties of reconstituted collagen fibers prior to self-assembly: animal species and collagen extraction method *J. Biomed. Mater. Res.* A **86** 892–904
[73] Capella-Monsonís H, Coentro J Q, Graceffa V, Wu Z and Zeugolis D I 2018 An experimental toolbox for characterization of mammalian collagen type I in biological specimens *Nat. Protocols* **13** 507–29
[74] O'Connor-Mccourt M, Sulea T, Zwaagstra J and Baardsnes J 2013 Antagonists of ligands and uses thereof, CA Nat Research Council
[75] Rao L V, Rao K T and Kandepi V V K M 2020 A novel validated UHPLC method for estimation of assay and its related substances of trichostatin-A *Int. J. Pharm. Sci.* **12** 45–50
[76] Ghanaeian A and Soheilifard R 2021 Comparative analysis of the viscoelastic properties of collagen-like proteins by virtual creep test *J. Biomol. Struct. Dyn.* **39** 2744–53
[77] Zeugolis D, Paul G and Attenburrow G 2009 Cross-linking of extruded collagen fibers—a biomimetic three-dimensional scaffold for tissue engineering applications *J. Biomed. Mater. Res.* A **89** 895–908
[78] Sanami M *et al* 2015 Biophysical and biological characterisation of collagen/resilin-like protein composite fibres *Biomed. Mater.* **10** 065005
[79] Sallent I, Capella-Monsonís H and Zeugolis D I 2019 Production and characterization of chemically cross-linked collagen scaffolds *Methods Mol. Biol.* **1944** 23–38
[80] Wu Z, Korntner S, Mullen A, Skoufos I, Tzora A and Zeugolis D 2021 In the quest of the optimal tissue source (porcine male and female articular, tracheal and auricular cartilage) for the development of collagen sponges for articular cartilage *Biomed. Eng. Adv.* **1** 100002
[81] Wu Z, Korntner S, Mullen A and Zeugolis D 2021 In the quest of the optimal chondrichthyan for the development of collagen sponges for articular cartilage *J. Sci. Adv. Mater. Devices* **6** 390–8
[82] Lotz C, Schmid F, Oechsle E, Monaghan M, Walles H and Groeber-Becker F 2017 Cross-linked collagen hydrogel matrix resisting contraction to facilitate full-thickness skin equivalents *ACS Appl. Mater. Interfaces* **9** 20417–25
[83] Wu Z, Korntner S, Olijve J, Mullen A and Zeugolis D 2021 The influence of bloom index, endotoxin levels and polyethylene glycol succinimidyl glutarate crosslinking on the physicochemical and biological properties of gelatin biomaterials *Biomolecules* **11** 1003
[84] Wang Y, Wu Z, Liu B, Lu J, Tanumiharjo S, Huang J, Zhao X and Lu L 2021 Efficacy and safety of scleral crosslinking using poly(ethylene glycol)ether tetrasuccinimidyl glutarate for form-deprivation myopia progression in rabbits *RSC Adv.* **11** 31746–55
[85] Du X, Zhou J, Shi J and Xu B 2015 Supramolecular hydrogelators and hydrogels: from soft matter to molecular biomaterials *Chem. Rev.* **115** 13165–307
[86] Okay O 2000 Macroporous copolymer networks *Prog. Polym. Sci.* **25** 711–79
[87] Davis B K 1974 Diffusion of polymer gel implants *Proc. Natl Acad. Sci. USA* **71** 3120–3
[88] Wang Y 2018 Programmable hydrogels *Biomaterials* **178** 663–80
[89] Li J and Mooney D J 2016 Designing hydrogels for controlled drug delivery *Nat. Rev. Mater.* **1** 16071
[90] Lee S, Tong X and Yang F 2016 Effects of the poly(ethylene glycol) hydrogel crosslinking mechanism on protein release *Biomater. Sci.* **4** 405–11
[91] Hu Y, Hu S, Zhang S, Dong S, Hu J, Kang L and Yang X 2021 A double-layer hydrogel based on alginate-carboxymethyl cellulose and synthetic polymer as sustained drug delivery system *Sci. Rep.* **11** 9142
[92] van Doren S R 2015 Matrix metalloproteinase interactions with collagen and elastin *Matrix Biol.* **44–46** 224–31
[93] Kumar P, Satyam A, Cigognini D, Pandit A and Zeugolis D I 2018 Low oxygen tension and macromolecular crowding accelerate extracellular matrix deposition in human corneal fibroblast culture *J. Tissue Eng. Regen. Med.* **12** 6–18
[94] Madry H, Rey-Rico A, Venkatesan J K, Johnstone B and Cucchiarini M 2014 Transforming growth factor beta-releasing scaffolds for cartilage tissue engineering *Tissue Eng.* B **20** 106–25
[95] Wakefield L M, Winokur T S, Hollands R S, Christopherson K, Levinson A D and Sporn M B 1990 Recombinant latent transforming growth factor beta 1 has a longer plasma half-life in rats than active transforming growth factor beta 1, and a different tissue distribution *J. Clin. Invest.* **86** 1976–84
[96] McCaffrey T A, Falcone D J, Vicente D, Du B, Consigli S and Borth W 1994 Protection of transforming growth factor-beta 1 activity by heparin and fucoidan *J. Cell. Physiol.* **159** 51–59
[97] Glue P, Fang J W, Rouzier-Panis R, Raffanel C, Sabo R, Gupta S K, Salfi M and Jacobs S 2000 Pegylated interferon-alpha2b: pharmacokinetics, pharmacodynamics, safety, and preliminary efficacy data. Hepatitis C intervention therapy group *Clin. Pharmacol. Ther.* **68** 556–67
[98] Lichtman M K, Otero-Vinas M and Falanga V 2016 Transforming growth factor beta (TGF-β) isoforms in wound healing and fibrosis *Wound Repair Regen.* **24** 215–22
[99] Sarrazy V, Billet F, Micallef L, Coulomb B and Desmoulière A 2011 Mechanisms of pathological scarring: role of myofibroblasts and current developments *Wound Repair Regen.* **19** s10–5
[100] Gasca-Lozano L E *et al* 2017 Pirfenidone accelerates wound healing in chronic diabetic foot ulcers: a randomized, double-blind controlled trial *J. Diabetes Res.* **2017** 3159798
[101] Zhang J B, Li H, Zhang L and Wang J L 2019 Observation of curative effect of recombinant human basic fibroblast growth factor combined with compound polymyxin B ointment and local application of insulin on wound healing of deep second-degree burn in diabetes mellitus: a randomized study *Eur. Rev. Med. Pharmacol. Sci.* **23** 5987–93
[102] Yarahmadi A, Saeed Modaghegh M H, Mostafavi-Pour Z, Azarpira N, Mousavian A, Bonakdaran S, Jarahi L, Samadi A, Peimani M and Hamidi Alamdari D 2021 The effect of platelet-rich plasma-fibrin glue dressing in combination with oral vitamin E and C for treatment of non-healing diabetic foot ulcers: a randomized, double-blind, parallel-group, clinical trial *Expert Opin. Biol. Ther.* **21** 687–96
[103] Panahi Y, Izadi M, Sayyadi N, Rezaee R, Jonaidi-Jafari N, Beiraghdar F, Zamani A and Sahebkar A 2015 Comparative trial of aloe vera/olive oil combination cream versus

phenytoin cream in the treatment of chronic wounds *J. Wound Care* **24** 459–60
[104] Gallelli G *et al* 2020 Nano-hydrogel embedded with quercetin and oleic acid as a new formulation in the treatment of diabetic foot ulcer: a pilot study *Int. Wound J.* **17** 485–90
[105] Chao T, Porter C, Herndon D N, Siopi A, Ideker H, Mlcak R P, Sidossis L S and Suman O E 2018 Propranolol and oxandrolone therapy accelerated muscle recovery in burned children *Med. Sci. Sports Exerc.* **50** 427–35
[106] Jeschke M G, Finnerty C C, Kulp G A, Przkora R, Mlcak R P and Herndon D N 2008 Combination of recombinant human growth hormone and propranolol decreases hypermetabolism and inflammation in severely burned children *Pediatr. Crit. Care Med.* **9** 209–16
[107] Herndon D *et al* 2018 Finnerty, reduced postburn hypertrophic scarring and improved physical recovery with yearlong administration of oxandrolone and propranolol *Ann. Surg.* **268** 431–41
[108] Norambuena C, Yañez J, Flores V, Puentes P, Carrasco P and Villena R 2013 Oral ketamine and midazolam for pediatric burn patients: a prospective, randomized, double-blind study *J. Pediatr. Surg.* **48** 629–34
[109] Jiang B, Zhang G and Brey E 2013 Dual delivery of chlorhexidine and platelet-derived growth factor-BB for enhanced wound healing and infection control *Acta Biomater.* **9** 4976–84
[110] Qu Y, Cao C, Wu Q, Huang A, Song Y, Li H, Zuo Y, Chu C, Li J and Man Y 2018 The dual delivery of KGF and bFGF by collagen membrane to promote skin wound healing *J. Tissue Eng. Regen. Med.* **12** 1508–18
[111] Vijayan A, A. S and Kumar G S V 2019 PEG grafted chitosan scaffold for dual growth factor delivery for enhanced wound healing *Sci. Rep.* **9** 19165
[112] Long G, Liu D, He X, Shen Y, Zhao Y, Hou X, Chen B, OuYang W, Dai J and Li X 2020 A dual functional collagen scaffold coordinates angiogenesis and inflammation for diabetic wound healing *Biomater. Sci.* **8** 6337–49
[113] Xie L, Ding X, Budry R and Mao G 2018 Layer-by-layer DNA films incorporating highly transfecting bioreducible poly(amido amine) and polyethylenimine for sequential gene delivery *Int. J. Nanomed.* **13** 4943–60
[114] Zou Y, Xie L, Carroll S, Muniz M, Gibson H, Wei W, Liu H and Mao G 2014 Layer-by-layer films with bioreducible and nonbioreducible polycations for sequential DNA release *Biomacromolecules* **15** 3965–75
[115] Gronowicz G, Jacobs E, Peng T, Zhu L, Hurley M and Kuhn L 2017 Calvarial bone regeneration is enhanced by sequential delivery of FGF-2 and BMP-2 from layer-by-layer coatings with a biomimetic calcium phosphate barrier layer *Tissue Eng.* A **23** 1490–501
[116] Guo H, Tan S, Gao J and Wang L 2020 Sequential release of drugs form a dual-delivery system based on pH-responsive nanofibrous mats towards wound care *J. Mater. Chem.* B **8** 1759–70
[117] Perez R, Kim J, Buitrago J, Wall I and Kim H 2015 Novel therapeutic core-shell hydrogel scaffolds with sequential delivery of cobalt and bone morphogenetic protein-2 for synergistic bone regeneration *Acta Biomater.* **23** 295–308
[118] Chen M, Cao H, Liu Y, Liu Y, Song F, Chen J, Zhang Q and Yang W 2017 Sequential delivery of chlorhexidine acetate and bFGF from PLGA-glycol chitosan core-shell microspheres *Colloids Surf.* B **151** 189–95